

# PV backsheets survey protocol: A framework for geo-spatial field surveys for bulk material characterization and reliability analysis applied across 41 PV systems

Raymond J. Wieser<sup>a</sup>, Zelin Li<sup>a</sup>, Xuanji Yu<sup>a</sup>, Stephanie L. Moffitt<sup>b</sup>, Ruben Zabalza<sup>c</sup>, Michael D. Kempe<sup>d</sup>, Liang Ji<sup>c</sup>, Colleen O'Brien<sup>c</sup>, Xiaohong Gu<sup>b</sup>, Kenneth P. Boyce<sup>c</sup>, Laura S. Bruckman<sup>a,\*</sup>

<sup>a</sup> SDLE Research Center, Case Western Reserve University, 10900 Euclid Ave., Cleveland, 44106, OH, USA

<sup>b</sup> Engineering Laboratory, NIST, Gaithersburg, 20899, MA, USA

<sup>c</sup> Underwriter's Laboratories Inc., Northbrook, 60062, IL, USA

<sup>d</sup> National Renewable Energy Laboratory, Golden, 80401, CO, USA

## ARTICLE INFO

### Keywords:

Photovoltaic array  
Field surveys  
Backsheet  
Degradation

## ABSTRACT

As widespread adoption of photovoltaic (PV) technologies continues, understanding the lifetime of modules is paramount to the viability of the industry as an environmentally conscious alternative to traditional energy generation. Although power degradation can affect the total energy production of a module over its lifetime, module safety failures necessitate the removal of a module leading to a loss of not only the particular asset, but the earning potential of the device. Therefore, it is critical to ensure that the components that provide essential safety functions for PV module operate for their entire rated lifetime. PV backsheets provide necessary electrical insulation to the completed device and failure of this component is cause for an immediate removal of the module. Degradation of the PV module backsheet has led to module safety failures in large-scale installations, costing millions of dollars in damages and lost potential revenue. The spatio-temporal degradation of fielded PV modules is important to study in order to identify which modules within installations are experiencing the greatest exposure conditions and in turn have the highest chance of failure. This paper describes a comprehensive field survey protocol developed for monitoring PV module backsheet performance using solely non-destructive methods in commercial PV fields. The protocol establishes a field naming convention, sampling method, data handling requirements, and measurement procedures. By ensuring consistent data collection practices, the field survey protocol enables research groups to obtain data of uniform quality on backsheet performance over multiple years and locations. In this study, the developed protocol was implemented at forty-one PV sites. Eight different types of airside layer backsheet materials including poly(vinylidene fluoride) (PVDF), acrylic PVDF, poly(tetrafluoroethylene-co-hexafluoropropylene-co-vinylidene fluoride) (THV), poly(vinyl fluoride) (PVF), poly(ethylene terephthalate) (PET), fluoroethylene vinyl ether (FEVE), polyethylene naphthalate (PEN), and glass were identified using attenuated total reflection Fourier transform infrared (ATR-FTIR) spectroscopy. The field survey results show that the spatial distribution of degradation indicators are non-uniform within a particular module, individual site, and across site locations. The degradation of PV modules increased in severity for modules mounted at the edge of rows (across a field) and near the junction box (within a module). This study demonstrates the sensitivity of material performance to exposure length across different materials and climates.

## 1. Introduction

Global installation of PV modules surpassed 444GW installed capacity in 2023, representing a 76% increase from the previous year [1]. In the United States, PV systems have surpassed 142.3 gigawatts-direct

current ( $GW_{dc}$ ) of installed capacity [2]. Meanwhile, solar PV energy costs are rapidly declining [3]. PV represents one of the most critical alternative energy technologies to replace non-renewable energy sources. PV power is more stable than other renewable energy technologies, such as wind energy and hydropower, especially because

\* Corresponding author.

E-mail address: [lsh41@case.edu](mailto:lsh41@case.edu) (L.S. Bruckman).

<https://doi.org/10.1016/j.solener.2025.113346>

Received 3 September 2024; Received in revised form 6 January 2025; Accepted 11 February 2025

Available online 13 March 2025

0038-092X/© 2025 The Authors. Published by Elsevier Ltd on behalf of International Solar Energy Society. This is an open access article under the CC BY-NC-ND license (<http://creativecommons.org/licenses/by-nc-nd/4.0/>).

of the projected large variability in power generation caused by global climate change [4,5]. However, the reliability of PV modules in the field is crucial for furthering solar energy development and controlling costs [6]. Preventative maintenance in the field serves to lower the risk of module failure and help research institutions to improve the protocols of lab-accelerated aging tests.

Extensive research has been conducted on the degradation of PV cells and encapsulants [7], but the importance of considering the degradation of the backsheets in PV modules cannot be disregarded. Backsheets are subject to a variety of synergistic stressors, including but not limited to humidity, temperature, irradiance, and wind speed [8–17]. Additionally, the rapidly changing climate is leading to larger variations in climatic stressors and an overall increase of high energy UV radiation [18]. The airside layer of backsheets commonly experiences degradation, which can result in yellowing and cracking [16]. Cracks in the polymer backsheets can lead to electrical isolation loss, leading to a module safety failure. Thus, Yellowness Index (YI) would be considered as a proxy indicator of the extent of backsheets degradation and cracks could be considered as a qualitative indicator.

Field surveys of outdoor exposed modules provide the most accurate information of long term material performance [19–22]. These surveys provide a visual and direct method to assess the extent of PV module degradation. However, these surveys usually sample modules sporadically without attention to the local environment around the sample or rely on destructive analysis of retrieved modules [16,21,23]. Most importantly, it is not feasible to pause product development to test the long term durability of emergent technologies in the field. Accelerated aging studies seek to replicate outdoor exposure, characterized by a specific climatic exposure type, in a fraction of the time to streamline product development but have been shown to not accurately predict material failure [10], although developments in combining cycles of different exposure steps is being actively studied [24,25]. However, through the combination of field measurements and computational models, indoor and outdoor aging conditions can be correlated to better inform module construction and materials certification. [26–28]. The distribution of spatial and temporal backsheets degradation is typically non-uniform due to the influence of various micro-climatic effects [22,26,29]. These stressors introduce variability, resulting in diverse patterns of degradation across different locations and time periods. Fairbrother et al. showed that the architecture of the module array leads to differential backside irradiance of the modules (micro-climates) [29]. This was accompanied by larger values of degradation predictors in the sections with higher light exposure. Module shading and ground albedo were shown as the most important characteristics in determining the backside irradiance [29]. The difference in exposures will intensify over the lifetime of the module which will lead to a decrease in the overall power generation efficiency of the system due to overexposed panels.

This research investigates the degradation patterns of backsheets in operational photovoltaic power plants. To accomplish this, a comprehensive protocol for field surveys has been developed, refined and tested based on the input from domain experts (industry and research) and years of field survey experience. The protocol serves as a standardized guide for research groups conducting surveys at global sites, ensuring consistency in measurement methods and data formats for subsequent analysis. The protocol suggests using Köppen Geiger Climatic Zone (kgc) as an approximate indicator of local climate to inform site selection [30,31] although other PV climate classifications also exist [32,33]. The protocol can be adapted for a large variety of different field measurements, and provides a general guideline for conducting surveys to leverage spatial information. A total of 41 sites, spanning exposure times from 1 to 38 years, were surveyed following the established protocol. The results reveal a non-uniform spatial and temporal distribution of backsheets degradation. Additionally, the study explores the correlation between degradation and common system attributes such as mounting height, ground albedo, and the position of the junction box. Furthermore, the research compares the differences in backsheets degradation among different material types and across various climate zones.

## 2. Methods: Study protocol development

In order to ensure consistent data collection across different research groups and over time in PV systems, a protocol has been developed by this work. This protocol includes the terminology that was used in the sites, the standard operating procedure (SOP) of instruments, Gage Repeatability and Reproducibility (GR&R) of measurements and tools were required during the surveys. It also clarifies the number of measurements for the modules, subrows, rows, and sites. The protocol establishes a uniform data structure and naming convention for measurements from surveyed sites, which standardizes terminology and assets in the collection/curation of large amounts of survey data. In addition, a training video was developed for detailed instructions on how to properly conduct field surveys. Both documents and the video are shared to Open Science Framework (OSF) [34]. All of metadata, de-identified site data and measurements collected using this protocol are available on OSF [34].

### 2.1. Terminology

In order to create a standardized protocol, a standard lexicon of PV terms was established. The following terminology has been developed through a collaborative effort with leading field survey experts and industry leaders.

#### 2.1.1. 'Blocks'

PV field refers to a large-scale installation of PV panels or modules, including the entire system of one solar power plant. 'Blocks' are the large grouping of PV modules in one field and do not need to be the same shape between commercial fields since commercial power plants are frequently nonuniform in layout. They are physical grouping of rows of modules. They are used to roughly locate the region of the field where measurements were taken. Blocks may or may not have the same exposure conditions as other 'Blocks' in the field. Different 'Blocks' of modules may or may not have the same material type or be electrically connected. An overview of a PV field can be found in Fig. 1.

#### 2.1.2. 'Rows'

The term of 'Row', 'Rack', 'Subrow', and 'Module Number' are defined for the modules installed in the power plant, as shown in Fig. 2. 'Row' are continuous groupings of modules arranged in a line and do not need to be the same length. 'Rack' refers to a continuous set of modules without physical spacing between mounting structures. They are usually a continuous electrical strings of modules. 'Module Number' is defined to describe the position of modules in the 'Row'. An individual 'Row' can have more than one module mounted on top of each other. When a 'Row' has multiple modules mounted vertically (portrait or landscape), each 'Row' will receive a 'Subrow' designation. Modules in 'Rows' can either be mounted at a constant angle or on single-axis tracker.

### 2.2. Effect size and sampling rate determination

In order to create representative models of backsheets degradation, a statistically significant portion of observations must be drawn from the population. The samples size can be determined based on the expense of data collection, and level of predetermined error probability. Thus, the sample size is a function of three predetermined factors,  $\alpha$  (Type I error probability),  $\beta$  (Type II error probability), and the desired effect size. This approach can then be applied to multiple linear regression models of historical field survey data to determine the actual number of samples needed to obtain the desired effect size [26]. The Cohen's  $f^2$  effect size for a multiple regression is defined as Eq (1) where  $R^2$  is the squared multiple correlation. A freely available software package called GPower was used to calculate the desired sample size [35,36].

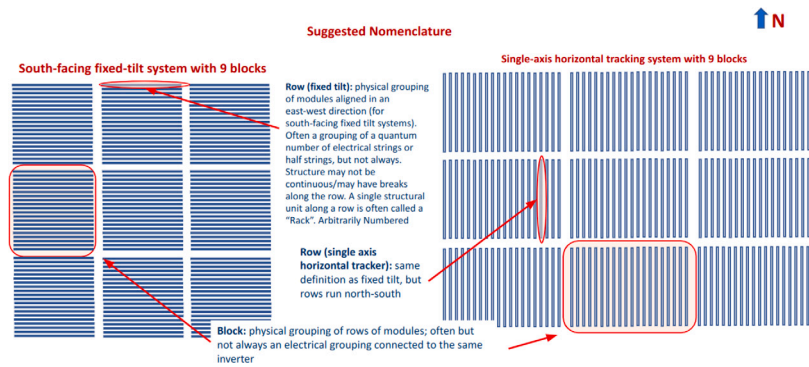


Fig. 1. Sketch of a photovoltaic field with individual 'Blocks', circled in red. Two different system layouts are shown: A south facing fixed tilt system, and a single axis tracking system with a north-south axis of rotation. The suggested nomenclature has been annotated on top of the diagram. (For interpretation of the references to color in this figure legend, the reader is referred to the web version of this article.)

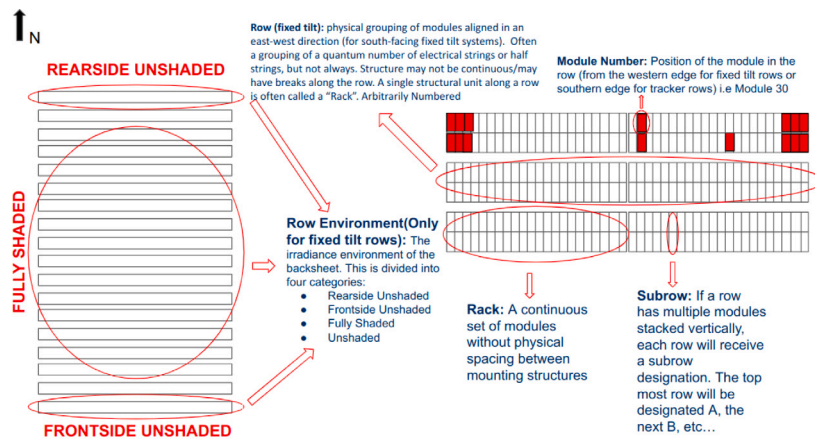


Fig. 2. A expanded view of the components that comprise a 'Block' of modules. The 'Block' of modules can be sub-divided into different Row Environments, Rows, Racks, Subrows, and Modules.

**Table 1**  
Sample sizes for measurement instruments, Yellowness Index (YI) and gloss calculated with a statistical power ( $d$ ) of  $d = 0.8$  [35,36].

	YI	Gloss
$\alpha$	.05	.05
$\sigma$	0.2	2
Effect Size	0.4	0.5
Sample Size	135	99

The sample size calculation for different statistical powers can be found in Table 1.

$$f^2 = \frac{R^2}{1 - R^2} \tag{1}$$

### 2.3. Visual inspection

Before conducting measurements with the field instrumentation, a visual inspection will be completed for the whole field. This inspection will assist in the survey team's understanding of the site, provide insights into locations to survey, and alert the survey team to any safety concerns. Observations from the visual inspection should be recorded with the location of the defects to better understand the spatial distributions of visual defects.

### 2.4. Instrumentation

Attenuated total reflection Fourier transform infrared (ATR-FTIR) spectroscopy is used to identify the airside material of backsheets. It is measured for each module with an Agilent 4300 handheld FTIR Spectrometer with diamond tip from  $4000\text{cm}^{-1}$  to  $650\text{cm}^{-1}$ . The materials are confirmed by comparing with the reference spectrum and other research on various materials [27,29,37-46].

HunterLabs MiniScan EZ 4000L with diffuse/ $8^\circ$  geometry is used to measure the YI. YI was calculated using the ASTM E313 standard [47].

Gloss measurements indicate the surface roughness of a material, a property that changes overtime in response to material aging. Gloss measurements are based on the standard ASTM D2457 [48]. BYK Micro-TRI-gloss was used for gloss measurements. It combines  $20^\circ$ ,  $60^\circ$  and  $85^\circ$  three angles in one instrument. The values of  $60^\circ$  are more stable and have less variance than the other two geometries. Thus,  $60^\circ$  geometry is used as the degradation predictor for this study.

### 2.5. Measurement number, position and order

Row and module selection depends on the research focus. Two types of sampling will be conducted during surveys: statistical and observational. The statistical sampling will focus on the condition of the modules as a whole. Although, the exposure environment varies based on the specific site being surveyed, it can be generally assumed that there will be a 'Row' of modules with an unshaded backsheets, one 'Row' with complete shading, and one 'Row' of only backsides shading. The statistically informed sampling procedure should be used to collect measurements to cover these criteria. The number of 'Rows' to survey

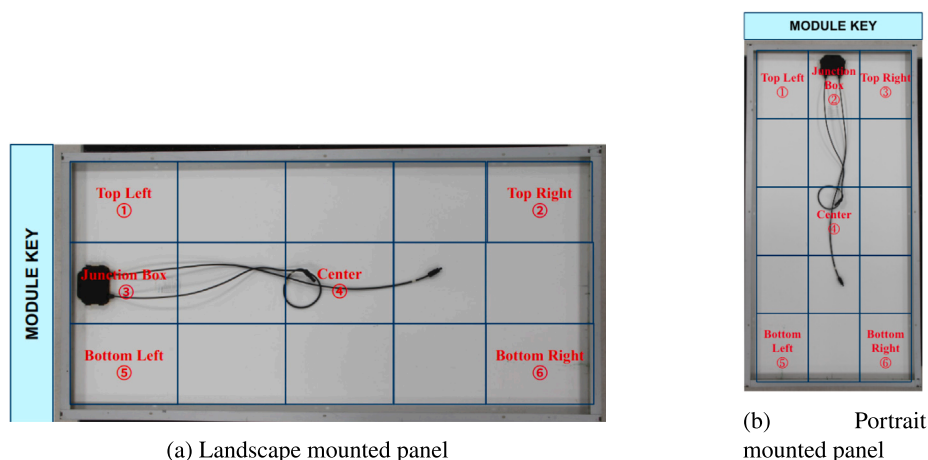


Fig. 3. Suggested measurement positions and order for either Landscape or Portrait module mounting configurations. (a) Proposed measurement locations for a landscape mounted panel. (b) Proposed measurement locations for a portrait mounted panel.

will vary with site layout, but in general triplicate measurements on each type of environment are preferred. A experienced survey team of two members can manage to measure 24–36 modules per hour depending on the size of the installation and the spacing of the measurements. FTIR measurement takes the longest and is the most difficult to get a clear reading of the material spectra. A survey team can consist of two researchers, one operating the FTIR, the other operating the Colorimeter and the Gloss meter. Additional team members can take other measurements on the site architecture, write down notes from the visual inspections or collect other/more measurements using different/the same instruments. Typical surveys measured approximately 144 modules divided evenly among the ‘Rows’ and ‘Subrows’ sampling different material varieties if the information was known. For a typical ‘Row’ of modules (20–50 modules per ‘Row’) the protocol recommends to measure 12 modules, 6 on the rack ends, and 6 in the rack center (spaced evenly). If a module ‘Row’ has multiple modules mounted on top of each other, this protocol suggests to measure each levels with the same frequency and at the same locations. Observational sampling will be conducted on modules of interest (i.e., modules that display random defects). This observational sampling can include modules with hotspots, cracks, delamination, etc.

For the position of each module, this protocol recommends at least six measurements for quantitative analysis and one to two measurements for qualitative analysis. For quantitative analysis, six or more measurements should be taken in the order of top left, close to the junction box, top right, center, bottom left, and bottom right (Fig. 3). In qualitative analysis, the measurements should be located near the center of the modules. An additional measurement is recommended near the junction box. The number of measurements is informed from measured field data and the effect size determination in Section 2.2.

### 3. Results

#### 3.1. Overview

In this research, a total of 41 sites were surveyed, consisting of 40 sites located in different states within the United States, and an additional international site in Taiwan. The international site was surveyed by another team, following the provided protocol documents and instructional videos. Along with the measurements taken in the field, fielded modules were obtained whenever possible for destructive characterization. The age of the surveyed solar power plants ranged from 1 year to 38 years, with the majority of sites being less than 10 years old. Most of the sites had a generated power capacity smaller than 1 MW. Detailed information for all sites can be found in Table 2, which encompasses seven different climate zones and eight different



Fig. 4. Rear side photo of modules was taken from the site located in Portland. The surface of the backsheet has been contaminated by biological materials.

materials. Additionally, Table 3 presents the total number of modules and surveys conducted for each backsheet material and their respective Köppen Geiger Climatic zone [30]. Eight different types of airside layer backsheet materials including poly(vinylidene fluoride) (PVDF), acrylic PVDF, poly(tetrafluoroethylene-co-hexafluoropropylene-co-vinylidene fluoride) (THV), poly(vinyl fluoride) (PVF), poly(ethylene terephthalate) (PET), fluoroethylene vinyl ether (FEVE), polyethylene naphthalate (PEN), and glass were identified using attenuated total reflection Fourier transform infrared (ATR-FTIR) spectroscopy. The survey team was unable to conduct surveys on fields with known PA backsheets due to safety considerations, but were able to collect a fielded module (Cfa 5yrs Exposure) with PA backsheet.

#### 3.2. Visual inspection

Several observational features were identified during the field visual inspection of the PV site and are described here. The visual inspection showed accumulation of soilage, vegetation, insect eggs, avian nests, bee colonies, among other biological entities on the backsheets in the field surveys. Fig. 4 shows a soiled module observed from the site located in Portland.

Fig. 5 displays micro-cracks observed on PEN backsheets of modules from the Maryland site (SS-16-8). These micro-cracks were present during the survey conducted after ten years of exposure, but were absent during previous surveys of the same site (2016 and 2020 years). It is noteworthy that all modules exhibiting micro-cracks were located at the edges of the top ‘Subrow’. For all other materials, no visible cracks were observed during visual inspection, although some retrieved

**Table 2**

The information of field surveys has been completed in this work (40 sites in the United States and 1 site in Taiwan, ROC. Sites labeled SS-17-2 and SS-19-5 are regional testing facilities that have multiple different technologies under exposure for various lengths of time.)

Site Name	Backsheet Materials	Size	Age (Years)	Climate Zone	State/Region	Measured Modules
IN-01-1	Acrylic PVDF	1–5 MW	10.838	Am	Taiwan	54
SS-15-1	Acrylic PVDF	20 MW–25 MW	1.419	Cfa	SC	60
SS-15-2	FEVE	10–15 MW	1.416	Cfa	SC	60
SS-15-3	FEVE	5–10 MW	1.422	Cfa	SC	68
SS-15-4	Acrylic PVDF	1–5 MW	1.830	Cfa	TN	184
SS-16-0	PEN	<1 MW	4.173	Cfa	MD	201
SS-16-1	PEN	<1 MW	8.329	Cfa	MD	201
SS-16-2	Acrylic PVDF	1–5 MW	1.578	Cfa	MD	216
SS-16-3	Acrylic PVDF	1–5 MW	9.110	BSk	CO	72
SS-16-4	PVF	1–5 MW	6.868	Csb	CA	188
SS-16-5	Acrylic PVDF	1–5 MW	9.619	Csa	CA	72
SS-16-6	PET	1–5 MW	7.589	Csa	CA	72
SS-16-7	Acrylic PVDF	1–5 MW	3.458	Cfa	MD	216
SS-16-8	PEN	<1 MW	10.214	Cfa	MD	222
SS-17-1	PET	1 MW	5.184	Cfa/Dfa	OH	160
SS-17-2	Varies	<1MW	7.184	Cfa/Dfa	OH	21
SS-17-3	PET	1 MW	Varies	Cfa/Dfa	OH	224
SS-18-1	FEVE	<1 MW	10.734	Dfa	IL	32
SS-18-2	FEVE	<1 MW	10.734	Dfa	IL	48
SS-18-3	FEVE	<1 MW	12.704	Dfa	IL	72
SS-19-1	PVF	<1 MW	6.910	Cfa	FL	24
SS-19-2	PET	<1 MW	6.910	Cfa	FL	32
	PVF					16
SS-19-3	PVDF	<1 MW	6.910	Cfa	FL	26
	THV					2
SS-19-4	THV	<1 MW	6.910	Cfa	FL	26
SS-19-5	Varies	<1 MW	Varies	Cfa	FL	20
SS-20-1	PVDF	<1 MW	14.773	Cfa	MA	36
SS-20-2	PVF	<1 MW	38.789	Cfa	MA	160
SS-21-1	PET	<1 MW	2.247	BSk	NM	30
SS-21-10	PET	<1 MW	2.589	BSk	NM	24
SS-21-2	THV	<1 MW	6.753	BSk	NM	28
SS-21-3	Acrylic PVDF	<1 MW	4.167	BSk	NM	24
SS-21-4	Acrylic PVDF	<1 MW	4.167	BSk	NM	24
SS-21-5	PET	<1 MW	3.586	BSk	NM	24
SS-21-6	PET	<1 MW	3.586	BSk	NM	24
SS-21-7	PET	<1 MW	4.167	BSk	NM	24
SS-21-8	PET	<1 MW	4.167	BSk	NM	24
SS-21-9	PVF	<1 MW	5.170	BSk	NM	24
SS-22-1	PVF	<1 MW	12.419	Csb	OR	96
SS-22-2	Glass	<1 MW	7.025	Csb	OR	60
SS-23-1	PET	1–5 MW	5.679	Dfb	MN	96
SS-23-2	FEVE	1–5 MW	6.600	Dfa	MN	180

modules that were collected exhibited backsheet cracking (Fig. 6). The retrieved modules (5yrs exposure, Cfa, PA Backsheet) exhibits deep longitudinal cracks.

Fig. 6 shows a visible degradation difference between sections near the junction box and other sections from a retrieved module collected from the commercial power plant. The backsheet color highlighted in the blue box is more yellow than the other sections of the modules.

### 3.3. ATR-FTIR

ATR-FTIR results are used to determine the backsheet materials. Samples were compared to FTIR reference spectrums for poly(vinylidene fluoride) (PVDF), acrylic PVDF, poly(tetrafluoroethylene-co-hexafluoropropylene-co-vinylidene fluoride) (THV), poly(vinyl fluoride) (PVF), two types of poly(ethylene terephthalate) (PET), fluoroethylene vinyl ether (FEVE) and polyamide (PA). PET with coating and PA were not present in any of the surveyed fields, but a fielded PA module was obtained for analysis. Seven different polymeric materials and one glass backsheet were identified from the FTIR analysis. The number of the samples for each material can be found in Table 3a.

Fig. 7 shows the FTIR spectrum comparison for two brands on the same site. Both backsheet materials were determined to be PET based. The spectrum is inconsistent at the lower wavenumbers, from  $600\text{ cm}^{-1}$



Fig. 5. Micro-cracks were observed from the site with ten years exposure. Site is located in Maryland within Cfa climate zone. The airside layer material is identified as PEN.

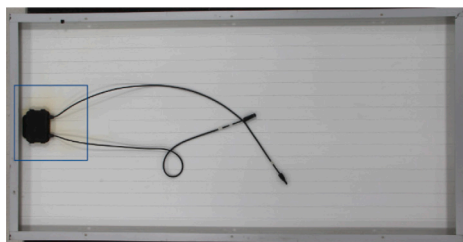
**Table 3**

(a) Number of modules and individual surveys for each air-side material identified through FTIR analysis (b) Number of modules and individual surveys for each Köppen Geiger Climate Zone in the dataset.

(a) Material types surveyed.		
Material Types	Surveys	Measured Modules
Acrylic	9	850
PVDF		
FEVE	6	460
PEN	3	624
PET	11	734
PVDF	2	134
PVF	6	508
THV	3	56
Glass	1	60

(b) Surveys by climatic zones.		
Climatic Zones	Surveys	Measured Modules
Am	1	54
Bsk	11	322
Cfa	19	2175
Csa	2	144
Csb	3	344
Dfa	7	737
Dfb	1	96



**Fig. 6.** A Retrieved Module after 5 years exposure in Cfa climate zone with PA outer-layer collected using the field survey protocol. The module displays non-uniform degradation and deep longitudinal cracks. The retrieved module has significant degradation near the junction box. This sample was obtained from a un-surveyed field, due to safety concerns.

to  $1250\text{ cm}^{-1}$ . Also, the ratio between some peaks is not consistent with the reference spectrum. It can be seen that the peak around  $1170\text{ cm}^{-1}$  has a significantly higher intensity in brand A, but not for the reference and brand B.

### 3.4. Yellowness index

Yellowness Index is a point in time measurement, and is used to characterize a specific sample at the time of measurement. By measuring multiple values of Yellowness Index across different materials and exposures, relative comparisons can be made based of the length of exposure and its severity. This makes Yellowness Index a useful proxy for measuring the severity of degradation. However, to make exact use of this information, a unexposed sample of the exact fielded material would be needed for comparison [23]. By aggregating large amounts of measurements while accurately describing the exposure of the material that lead to its current condition (in something like a field survey protocol), comparative studies of degradation can be conducted comparing the relative change in the severity of different exposures and change in each materials relative performance measured in Yellowness Index. Prior to analysis, the YI data was preprocessed to remove erroneous measurements and signals from biological contaminants. The values beyond  $\pm 3$  standard deviations (SD) from the mean for each 'Row'

were considered to be outliers and have been removed from analysis, but they are retained in the publicly available dataset. Generally, there will be 6 measurements for each module based on the protocol. In this research, we have YI data from 3,467 modules across all 41 surveys. Significant non-uniformity was found in the spatial distribution of YI values.

**Fig. 8** shows the range of YI for all the material identified from the surveys, colored by the climatic zone the materials was exposed under. The total range of YI are from  $-8$  to  $25$ , where PEN has the highest value of YI and PET has the lowest values of YI. PET and PEN exhibit the largest range of YI values. None of the materials surveyed were exposed in all of the observed climate zones.

**Fig. 9** illustrates the results of three site visits conducted in Maryland, which falls within the Cfa climate zone and a PEN based material backsheets. According to protocol, only a portion of the total 'Rows' and 'Subrows' needed to be measured, leaving empty plots when they are arranged in a spatial manner. In the case of **Row 5** and **Subrow B**, measurements were only taken during the surveys conducted after four years of exposure.

In **Row 1**, **Row 2**, **Row 3**, **Row 4** and **Subrow C**, **Subrow D**, **Subrow E**, the edge modules, the modules in the red box, exhibited YI values roughly  $2 - 5$  units higher than those of the middle modules or 'Rows'. As the exposure time increased, the YI values showed a more significant increase between four years of exposure and eight years of exposure, compared to the increase between eight years of exposure and ten years of exposure. After four years of exposure, 'Subrow' 'A' displayed an average YI value of approximately  $20$ , which was higher than the average YI value of  $15$  observed in **Subrow C**, **Subrow D**, and **Subrow E**. Over time, the difference between the edge modules and middle modules in each 'Row' decreased. After ten years of exposure, the YI of the edge modules in **Subrow A** had lower YI than the middle modules, which is contrary to the previous field survey results, and the other measurements in the same survey. Cracking was only observed on these anomalous edge modules (**Fig. 5**)

A heatmap was utilized to depict the YI values in their respective measurement locations for each 'Row', as shown in **Fig. 10**. These results were obtained from the site SS-17-3, which falls within the Cfa or Dfa climate zone. The backsheets measured in these surveys were composed of PET material. Each small box within the figure represents the results of six measurements taken from a single module. The YI values range from  $-1.5$  to  $0$ .

From the view of the 'Rows', it is evident that **Module 1**, **Module 2**, and **Module 3** exhibit higher YI values compared to the modules in the middle of the 'Row'. Additionally, within **Subrow A**, the top position displays a higher YI value in comparison to the bottom position of **Subrow B**. From the view of each modules, the measurements closest to the junction box are typically located either at the bottom middle or top middle of the modules. These measurements near the junction box consistently have higher YI values than other positions within each module, with the exception of certain modules located at the edges of the 'Row'.

**Fig. 11** shows the YI results obtained from a site where the ground coverage changes, along with a schematic of the map and the 'Row' arrangements. In the field layout map, the blue box represents an area where the ground is covered by grass. Conversely, the red box corresponds to an area with a ground cover consisting of gray stone. **Fig. 11(b)** illustrates the arrangement of 'Rows' and 'Subrows' at the site, progressing from **Subrow A** to **Subrow E** in decreasing order of clearance. **Fig. 11(c)** displays the YI results obtained from this site. Measurements made in gray stone ground cover area (red box) exhibits relatively higher YI values compared to grassy area (blue box). **Row 5** had dense weeds located behind the mounting rack, this 'Row' and its 'Subrows' exhibited the lowest YI values of the site.

**Fig. 12** shows the YI results obtained from SS-16-3 which had a non-uniform ground clearance, accompanied by corresponding schematics. In the YI results, the red box represents modules installed on a flat

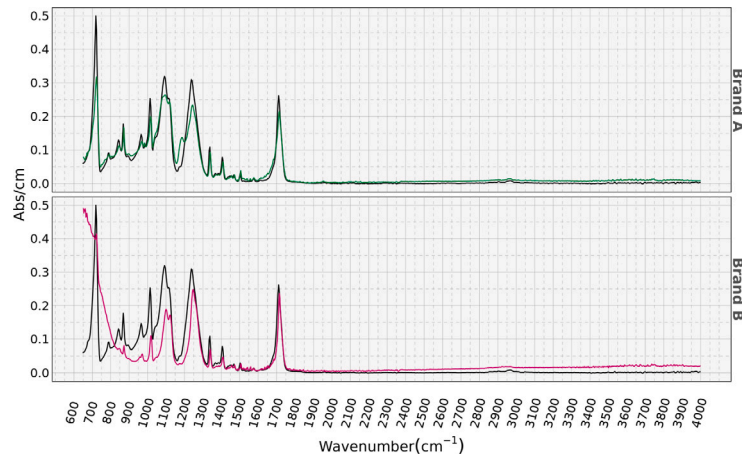


Fig. 7. A comparison of the ATR-FTIR spectra of PET from two different brands, obtained from the same site SS-17-3 within the Cfa or Dfa climate zone. The black line represents the reference spectrum of PET. The brand B spectra shows a strong absorbance near the lower wavenumbers most likely due to the absorbance of titania-dioxide fillers [49].

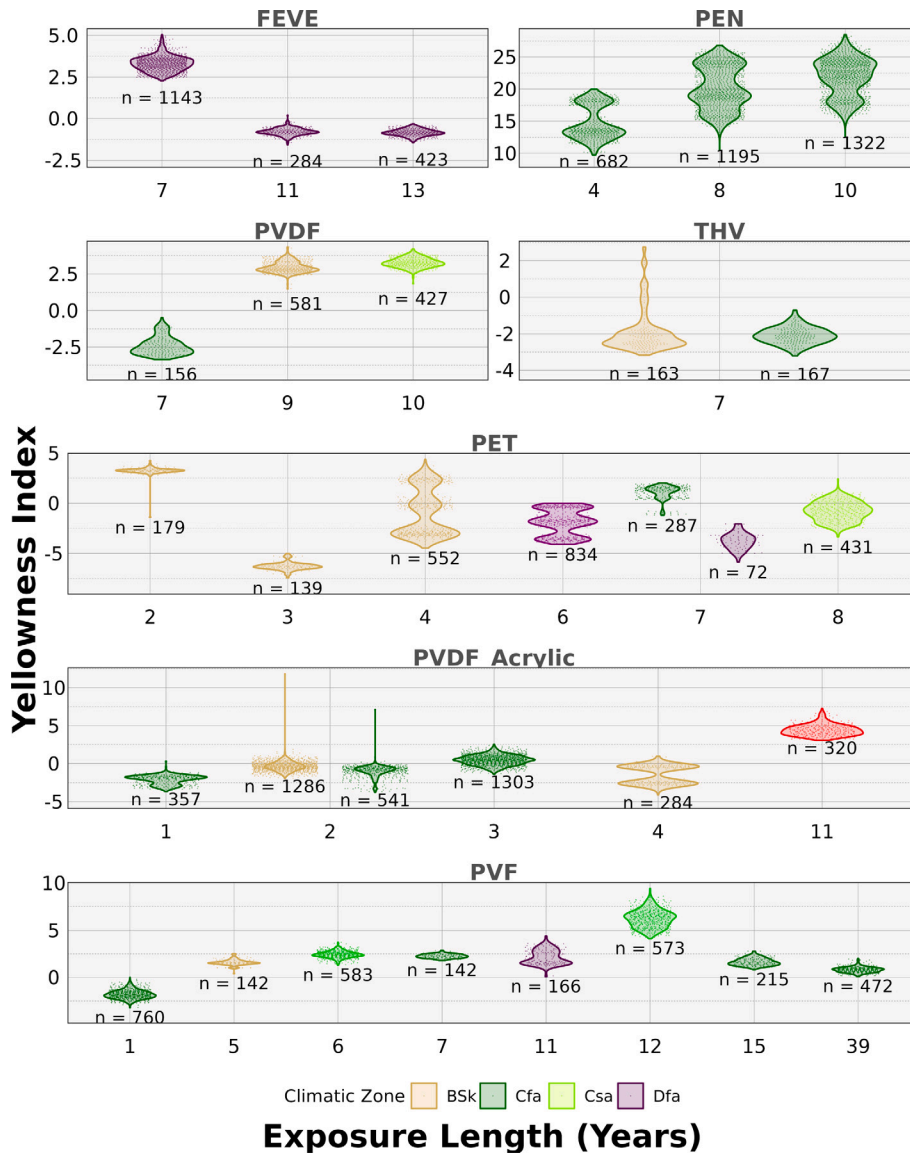
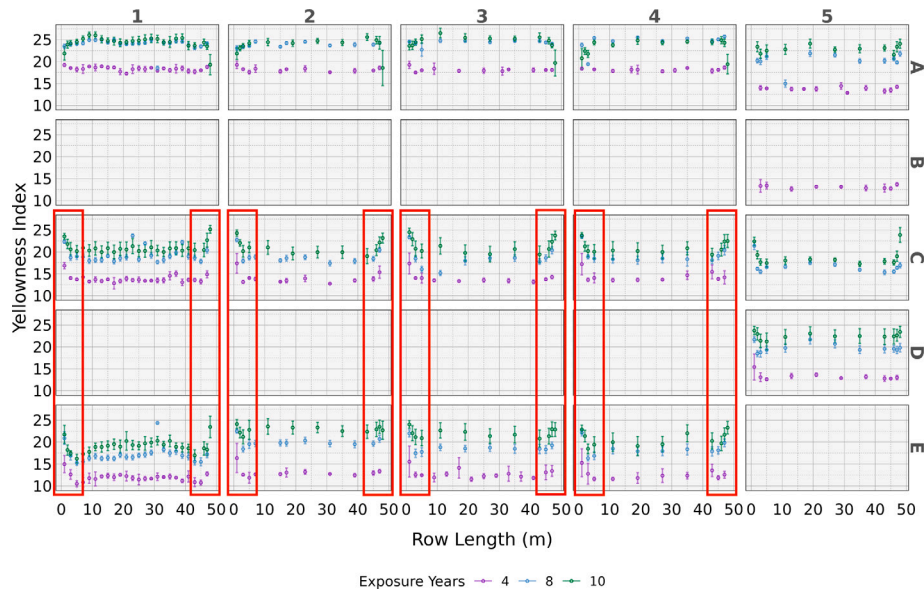
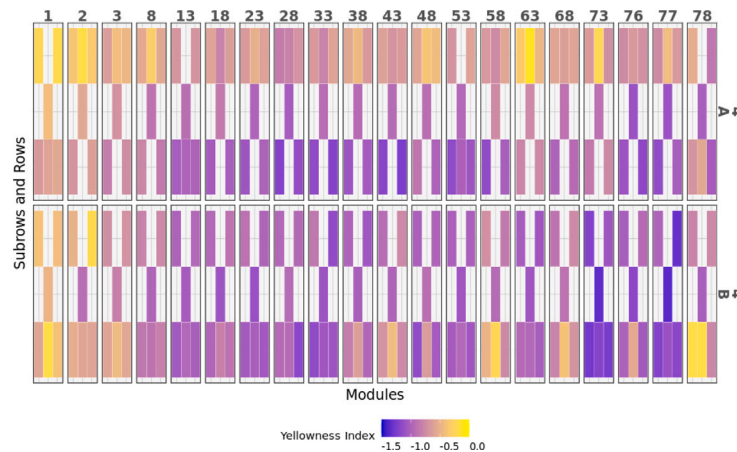


Fig. 8. The variation of YI over time for each material, derived from all surveys. The color represents the corresponding climate zone for each exposure duration. (For interpretation of the references to color in this figure legend, the reader is referred to the web version of this article.)



**Fig. 9.** Spatially distributed YI values for site in Maryland. Three separate visits were conducted at different times for site SS-16-8 with Cfa climate zone. The site was constructed in the year 2012. The red boxes highlight ‘Rows’ that exhibit a significant “Edge Effect” at this particular site. The horizontal axis represents the Row Length, while the vertical axis represents the ‘Subrow’. A vertical column represents one continuous mounting structure, whereas a horizontal column shows the variation of a single ‘Subrow’ across different ‘Rows’. A top down and side view of the site can be found in Fig. 11a & Fig. 11b. (For interpretation of the references to color in this figure legend, the reader is referred to the web version of this article.)



**Fig. 10.** The heatmap represents the YI values for Row ‘4’ obtained from the site located in Cleveland, Ohio within the Cfa or Dfa climate zone. The horizontal axis corresponds to the Module Name, while the vertical axis displays the ‘Subrow’ Name and Row Name. The measurements of YI have been arranged according to their measurement positions.

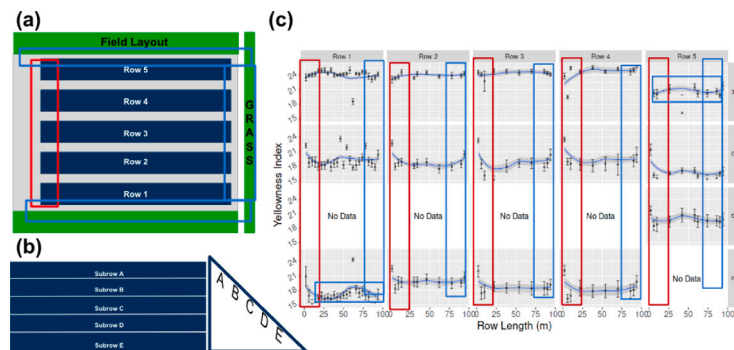


**Fig. 11.** The site SS-16-8 has a non-uniform albedo distribution. The site is located in Maryland within the Cfa climate zone. Red box has a high albedo ground. Blue box has a low albedo ground. (a) Schematic of field layout map. (b) Schematic of side view of the ‘Rows’, along with the corresponding ‘Subrow’ names. (c) YI results and spatial distribution, illustrating the degradation patterns across the site. (For interpretation of the references to color in this figure legend, the reader is referred to the web version of this article.)

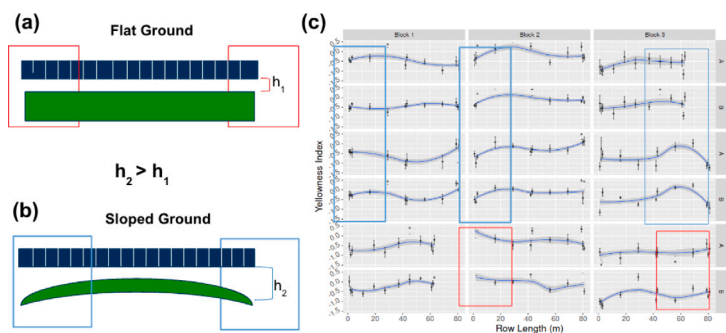


**Fig. 12.** The modules located in SS-16-7 were mounted on a uneven surface with significant changes in ground clearance within a ‘Row’. The site is located in Maryland within the Cfa climate zone. The red boxes indicate regions with flat ground. The blue boxes are regions with significant elevation changes. (a) Schematic of flat ground (b) Schematic of sloped ground (c) YI results and spatial distribution, illustrating the difference degradation patterns across the site. (For interpretation of the references to color in this figure legend, the reader is referred to the web version of this article.)

ground, while the blue box represents modules installed on a inclined surface. Fig. 12(c) displays the YI results obtained from this site. The modules mounted on a uniform section of ground with low clearance exhibited a greater YI than the same modules mounted with high ground clearance.

### 3.5. Gloss

Material gloss was measured in conjunction with yellowness index at the same measurement locations. For modules, the variance of gloss value at 60° was much larger than the results of YI. A similar trend to spatial YI distribution was observed in the gloss results. The gloss results also show a difference between measurements on edge modules and middle modules. Additionally, gloss measurements close to the junction box have a significant difference compared to the other measurement positions. This was observed in both fixed tilt and tracker mounting structures. The intra-module gloss variance was larger than the inter-‘Row’ gloss variance, making it difficult to establish correlations to particular exposure conditions.

## 4. Discussion

### 4.1. Backsheet variability

The study was unable to determine the airside materials of the installed modules before surveying due to lack of information of the bill of materials and metadata. In addition, the formulation for each backsheet material varies between different brands or even within batches of modules [23] (Fig. 7). This leads to a large variance in degradation predictors for the same bulk polymer, and is especially present in the many formulations of PET that were surveyed (Fig. 8) [22]. The discrepancies in measurements within a polymer can be attributed to differences in the ratio of the polymer components, chain length, structure, and the ratio or composition of additives [23,27]. The manufacturing process impacts the overall performance of the material in the in real-world.

Furthermore, the backsheets are made of laminated polymers rather than a single layer or can be multiple layers with the same polymer. The non-destructive methods used to characterize modules in this survey only measure the air-side layer of the backsheet and could not characterize the other layers or deeper into the samples. Although the current measurements were limited to surface characterization, the proposed field survey protocol can be extended to other types of survey equipment that could measure different degradation predictors within the backsheet, encapsulants or cells [50–52].

### 4.2. Material performance

The aging sensitivity of backsheet polymers varies, as shown in Fig. 8. Notably, certain fluoropolymers such as FEVE, PVF, and THV

exhibit a color change to blue rather than yellow after exposure, but is imperceptible to the naked eye [17,26]. Additionally, the fluoropolymers had a much smaller range of values, which could mean that they have exhibited little change from their unexposed state [39,53]. This can be attributed to the superior stability of fluoropolymers, stemming from their inherent resistance to UV radiation due to the robust carbon-fluorine bonds they possess [9,22]. On the other hand, PEN demonstrates the largest variance among surveys and displays a significant temporal degradation distribution, as depicted in Fig. 9. After 10 years of exposure, visible degradation is observed at the top edges of PEN modules, as shown in Fig. 5. This area is subjected to the highest exposure in the field. In comparison to other materials, PEN exhibits large variance and high susceptibility to color change in response to irradiation. Although PEN is not a commonly used material in silicon PV backsheets, its susceptibility to changes in exposure environment highlight the spatially anisotropic nature of degradation stressors, and could provide information on how similar materials may behave under lifetime exposure [26,29].

### 4.3. Climatic zone specific degradation

Given that most materials were only measured in a limited number of climate zones, it is challenging to compare the effects of different climate zones on degradation. Moreover, fluoropolymers are widely recognized for their exceptional resistance to aging, which makes it difficult to detect degradation across diverse climate zones, as depicted in Fig. 8. When comparing the degradation patterns among various climate zones and materials, it becomes evident that certain materials may not exhibit discernible differences in degradation behavior while other materials may be sensitive to these changes [31,31]. For example, a substantial variation is observed in the YI results of PVDF between the BSk and Cfa climate zones. However, for THV and PVDF with acrylic, the differences are found to be insignificant. While climate zone classification alone may not fully capture the nuances of different weather conditions, it does not negate the existence of weather-related influences on the degradation behavior of materials [22].

### 4.4. Spatially anisotropic degradation

Elevated edge degradation was observed for all materials and climatic zones, which will be referred to as ‘Edge Effect’. Edge effect was more significant for the fixed tilt systems. As shown in Fig. 9, the edges of the ‘Rows’ experienced higher values of degradation predictors than the middle of ‘Rows’.

The non-uniform distribution of irradiance may contribute to the ‘Edge Effect’. Due to the complex interactions between the racking structure, ground clearance and surface albedo, the irradiance reflected from the ground can vary significantly in a ‘Row’ and even within a single panel. For fixed tilt systems, the edge modules are subjected to higher total exposure due to the increase of intensity of light being

reflected from the unshaded ground located near the ends of 'Rows'. Conversely, modules mounted in the center of 'Rows' do not experience the same intensity of light, leading to an overall lower total exposure. Previous research on SS-16 found that the edge of 'Rows' experienced higher irradiance exposure than the middle of 'Row', when measured by an irradiance sensor [29].

The presence of unshaded ground could also lead to a similar effect for 'Rows' with multiple 'Subrows'. Modules mounted at the top most 'Subrow' have a higher amount of incident light being reflected from the ground (which is unshaded) behind the mounting structures than modules located in center 'Subrows'. Likewise, modules located on bottom 'Subrows' can have an increased exposure due to the reflection of light from the area in-front of 'Row'. These effects are mediated by the ground albedo that the modules are mounted on which changes the intensity and distribution of wavelengths that are reflected. All of these changes in exposure environment can cause distinct exposure conditions leading to non-uniform degradation observed in the field (Fig. 11).

Variable ground covering also affects the intensity of reflected light [29]. Most of the surveyed fields were covered with stone or grass, but the coverage and consistency of material varied from 'Row' to 'Row'. Additionally material specific properties not only affect the intensity of reflected light, but also the wavelength. For example, gray stone reflects more UV than the green grass, so modules installed on stone substrate will experience higher exposure than if they were installed on grass [54]. Fig. 11 shows the significance of changing the ground albedo on degradation predictors. In this site, the grass has a lower albedo, leading to less UV light incident on the modules at the right edge of 'Rows'. The ground cover on the left side of the array is comprised of gray rock, which has a higher UV albedo. The modules mounted over the high albedo gray rock have much higher degradation predictor values when compared to the modules mounted on the low albedo surface of grass. This effect is prominent for both the edge modules and for modules mounted in-front of foliage in "Row 5" (Fig. 11). These changes in ground albedo have led to distinct degradation behaviors across many of the surveyed sites and in the literature [26,29].

Non-uniform distances between ground and modules also effect the magnitude of exposure [55]. Larger distances from the ground to the backsheet surface allow for more light scattering, leading to a decrease in overall light intensity [56]. If the mount height of the edge modules is significantly higher than the middle modules of the 'Row', the "Edge Effect" will be less significant or even not be present. Fig. 12 compares the 'Rows' with different mount heights. For the 'Rows' with sloped ground, blue boxes in Fig. 12 show more prominent 'Edge Effect' than others. This regions correspond to areas with smaller ground clearances.

Materials differences can also affect the degree of anisotropy measured in the field. Stable materials are less sensitive to changes in their environment, which reduces the effects from non-uniform exposure conditions.

#### 4.5. Non-uniform module degradation

Spatially resolved measurement techniques showed non-uniform degradation within module, as evidenced by visual inspection and heat map results shown in Figs. 6 and 10, which has been noted in the literature [26,29,53] The location of the junction box was observed to have a significant impact on both YI and gloss results. The measurements near the junction box consistently exhibited more significant degradation predictors compared to other positions within the module, particularly for modules located in the middle of 'Rows'. Even in cases where the location of the junction box was inconsistent, the sections near the junction box still exhibited higher values of YI. This trend held true for both tracker and fixed tilt modules, indicating that the proximity to the junction box was a critical factor in degradation.

The higher degradation near the junction box can be attributed to the elevated temperature of the junction box during module operation, as suggested by previous studies [57]. The increased temperature likely accelerates the degradation process, leading to more pronounced effects on the backsheets in close proximity to the junction box. Edge modules experience the combined effect of elevated junction box temperature and the 'Edge Effect' and thus had a less significant difference than the center modules. The anisotropy in edge modules is dominated by the increased rear-side irradiance and thus has a lower variance compared to the modules in the middle of the rows.

#### 4.6. Spatio-temporal degradation patterns

The field study protocol enabled the repeat surveying of PV sites in a reproducible manner. By measuring the same modules in the field over the course of multiple years, this study observed the real world degradation of field aged modules and how it progresses not only in time, but as a function of the module's location in the field/mounting structure. Field surveys at SS-16-0, SS-16-1, SS-16-8 span 6 years of exposure, and represent the middle life of the system, measurements were conducted on the same modules in the same locations for all surveys. A prominent spatial anisotropy is noted across all 'Rows' and 'Subrows', where the edge modules exhibit higher YI than the middle modules. This behavior changed in **Subrow A** in the most recent field survey, where the YI of the edge modules seemed to saturate, and in some cases was lower than that of the middle modules. The decreased production of yellow chromophores and increase of photobleaching of the edge modules indicates a change in degradation mechanism in the material under extended exposure. **Subrow A** is believed to have the highest amount of exposure due to the relatively high amount of UV light incident on the top most row of modules 4.4. The micro-cracks observed during the visual inspection of the site were only located on edge modules in **Subrow A**, which indicates that the change in degradation mechanism from yellowing corresponds to emergent degradation modes in the material that lead to cracking under prolonged exposure. This behavior has been studied in indoor accelerated exposures, where after extended exposures (> 2500 h cyclic exposure) laminated coupons stopped increasing in YI which then lead to cracking of the material [58].

#### 4.7. Field survey protocol

Developing a comprehensive field survey protocol has significantly enhanced our understanding of various critical factors influencing photovoltaic (PV) material performance. This protocol enabled us to identify and analyze backsheets material variability, revealing how differences in material formulation impact backsheets longevity. Additionally, we gained valuable insights into material performance under diverse environmental conditions. By examining modules across different climatic zones with the same airside material, the protocol enables studies of the sensitivity of materials to changes in climatic exposure. The survey also highlighted spatially anisotropic nature of degradation, indicating that degradation rates can vary within different parts of the same 'Site' or 'Block' or 'Row' or 'SubRow' or even 'Module' due to changes in the local micro-climate around the material. We observed able to observe non-uniform module degradation in the field, which stresses the necessity of detailed, localized analysis and a limitation of lab accelerated aging. Lastly, the identification of spatio-temporal degradation patterns provided a deeper understanding of how degradation evolves over time and space. This protocol encompasses a broader view on how to develop a field study protocol and conduct field measurements, and is intended to be used for a variety of non-destructive field measurements for any type of survey data.

## 5. Conclusions

In this research, a robust and refined protocol for conducting spatially aware field surveys was developed, incorporating domain knowledge and field observations. This protocol establishes a standardized nomenclature for PV field surveys and serves as a statistically informed framework that can be generalized to other components of PV modules. It enables research groups to ensure the quality and quantity of collected data. Based on the results obtained from a total of 41 surveys, both spatial and temporal degradation patterns were observed. Specifically, the sections near the junction box exhibited greater degradation compared to other sections, attributed to accelerated polymer aging caused by heat dissipation from the junction box. Furthermore, modules located at the edges of 'Rows' demonstrated higher levels of degradation, known as the 'Edge Effect'. This effect is influenced by various micro-climatic factors, including non-uniform UV distributions, mounting configuration, mount height, and variability in ground cover. It was observed that PEN exhibited the highest sensitivity to exposure, while most fluoropolymers displayed lower sensitivity. Moreover, comparing the behavior of materials across various climate zones revealed inconsistent trends, suggesting that macro-climate alone may not provide sufficient weather information for comprehensive backsheet degradation analysis. These observations highlight the non-uniform degradation experienced by fielded modules, offering a more comprehensive understanding than accelerated testing alone.

### CRediT authorship contribution statement

**Raymond J. Wieser:** Writing – review & editing, Writing – original draft, Visualization, Validation, Software, Project administration, Methodology, Investigation, Formal analysis, Data curation, Conceptualization. **Zelin Li:** Writing – original draft, Visualization, Formal analysis, Data curation. **Stephanie L. Moffitt:** Writing – review & editing, Resources. **Ruben Zabalza:** Resources. **Michael D. Kempe:** Resources. **Liang Ji:** Resources. **Colleen O'Brien:** Resources. **Xiaohong Gu:** Writing – review & editing, Resources. **Kenneth P. Boyce:** Project administration, Funding acquisition. **Laura S. Bruckman:** Writing – review & editing, Supervision, Resources, Project administration, Conceptualization.

### Declaration of Generative AI and AI-assisted technologies in the writing process

During the preparation of this work the author(s) used ChatGPT 3/4 in order to assist in readability and language. After using this tool/service, the author(s) reviewed and edited the content as needed and take(s) full responsibility for the content of the publication.

### Disclaimer

NIST disclaimer: Certain commercial products or equipment are described in this paper to specify adequate experimental procedures. In no case does such identification imply recommendation or endorsement by the NIST, nor does it imply that it is necessarily the best available for the purpose.

### Funding

This work was authored in part by the National Renewable Energy Laboratory, operated by Alliance for Sustainable Energy, LLC, for the U.S. Department of Energy (DOE) under Contract No. DE-AC36-08GO28308. Funding provided by the U.S. Department of Energy Office of Energy Efficiency and Renewable Energy Solar Energy Technologies Office. The views expressed in the article do not necessarily represent the views of the DOE or the U.S. Government. The U.S. Government retains and the publisher, by accepting the article for publication, acknowledges that the U.S. Government retains a nonexclusive, paid-up, irrevocable, worldwide license to publish or reproduce the published form of this work, or allow others to do so, for U.S. Government purposes.

## Declaration of competing interest

The authors declare that they have no known competing financial interests or personal relationships that could have appeared to influence the work reported in this paper.

## Acknowledgments

This material is based upon work supported by the U.S. Department of Energy's Office of Energy Efficiency and Renewable Energy (EERE) under Solar Energy Technologies Office (SETO) Agreement Number DE-EE-0008748. The views expressed herein do not necessarily represent the views of the U.S. Department of Energy or the United States Government. This work made use of the Rider High Performance Computing Resource in the Core Facility for Advanced Research Computing at Case Western Reserve University. The authors would like to acknowledge the hard work and dedication of the field survey team that took the thousands of measurements used in this study. Karissa Jensen and Song-Syun Jhang for helping collect field survey data.

## References

- [1] Bloomberg, 1Q 2024 global PV market outlook, BloombergNEF (2024-03-26).
- [2] SEIA/Wood Mackenzie Power & Renewables, Solar Market Insight Report 2022 Year in Review, Technical Report, 2023, URL: <https://www.seia.org/research-resources/solar-market-insight-report-2022-year-review>.
- [3] IRENA, Renewable power generation costs in 2021, 2021.
- [4] M.A. Russo, D. Carvalho, N. Martins, A. Monteiro, Forecasting the inevitable: A review on the impacts of climate change on renewable energy resources, *Sustain. Energy Technol. Assessments* 52 (2022) 102283, <http://dx.doi.org/10.1016/j.seta.2022.102283>, URL: <https://www.sciencedirect.com/science/article/pii/S2213138822003356>.
- [5] A.I. Osman, L. Chen, M. Yang, G. Msigwa, M. Farghali, S. Fawzy, D.W. Rooney, P.S. Yap, Cost, environmental impact, and resilience of renewable energy under a changing climate: a review, *Environ. Chem. Lett.* (2022) <http://dx.doi.org/10.1007/s10311-022-01532-8>.
- [6] R.A. Kharait, P. Stiles, J. Carriere, L. McClung, Impact of degradation rates on solar PV financing for projects located in the united states, in: 2017 IEEE 44th Photovoltaic Specialist Conference, PVSC, 2017, pp. 2833–2835, <http://dx.doi.org/10.1109/PVSC.2017.8366032>.
- [7] R. Dubey, S. Chattopadhyay, S. Zachariah, S. Rambabu, H.K. Singh, A. Kottantharayil, B.M. Arora, K. Narasimhan, N. Shiradkar, J. Vasi, On-site electroluminescence study of field-aged PV modules, in: 2018 IEEE 7th World Conference on Photovoltaic Energy Conversion (WCPEC) (a Joint Conference of 45th IEEE PVSC, 28th PVSEC & 34th EU PVSEC), (ISSN: 0160-8371) 2018, pp. 0098–0102, <http://dx.doi.org/10.1109/PVSC.2018.8548080>.
- [8] J.W. Zhang, W. Deng, Z. Ye, S. Diahm, C. Putson, X. Zhou, J. Hu, Z. Yin, R. Jia, Aging phenomena of backsheet materials of photovoltaic systems for future zero-carbon energy and the improvement pathway, *J. Mater. Sci. Technol.* 153 (2023) 106–119, <http://dx.doi.org/10.1016/j.jmst.2022.12.063>, URL: <https://www.sciencedirect.com/science/article/pii/S1005030223001664>.
- [9] W. Gambogi, Y. Heta, K. Hashimoto, J. Kopchick, T. Felder, S. MacMaster, A. Bradley, B. Hamzavtehrany, L. Garreau-Iles, T. Aoki, K. Stika, T.J. Trout, T. Sample, A comparison of key PV backsheet and module performance from fielded module exposures and accelerated tests, *IEEE J. Photovoltaics* 4 (3) (2014) 935–941, <http://dx.doi.org/10.1109/JPHOTOV.2014.2305472>, Conference Name: IEEE Journal of Photovoltaics.
- [10] Y. Lyu, J.H. Kim, A. Fairbrother, X. Gu, Degradation and cracking behavior of polyamide-based backsheets subjected to sequential fragmentation test, *IEEE J. Photovoltaics* 8 (6) (2018) 1748–1753, <http://dx.doi.org/10.1109/JPHOTOV.2018.2863789>, Conference Name: IEEE Journal of Photovoltaics.
- [11] C.C. Lin, Y. Lyu, L.C. Yu, X. Gu, Correlation between mechanical and chemical degradation after outdoor and accelerated laboratory aging for multilayer photovoltaic backsheets, in: Reliability of Photovoltaic Cells, Modules, Components, and Systems IX, vol. 9938, SPIE, 2016, pp. 57–67, <http://dx.doi.org/10.1117/12.2238216>, URL: <https://www.spiedigitallibrary.org/conference-proceedings-of-spie/9938/99380H/Correlation-between-mechanical-and-chemical-degradation-after-outdoor-and-accelerated/10.1117/12.2238216.full>.
- [12] A. Omazic, G. Oreski, M. Halwachs, G.C. Eder, C. Hirschl, L. Neumaier, G. Pinter, M. Erceg, Relation between degradation of polymeric components in crystalline silicon PV module and climatic conditions: A literature review, *Sol. Energy Mater. Sol. Cells* 192 (2019) 123–133, <http://dx.doi.org/10.1016/j.solmat.2018.12.027>, URL: <https://www.sciencedirect.com/science/article/pii/S0927024818305956>.

- [13] M.D. Kempe, J.H. Wohlgemuth, Evaluation of temperature and humidity on PV module component degradation, in: 2013 IEEE 39th Photovoltaic Specialists Conference, PVSC, (ISSN: 0160-8371) 2013, pp. 0120–0125, <http://dx.doi.org/10.1109/PVSC.2013.6744112>.
- [14] E. Wang, H.E. Yang, J. Yen, S. Chi, C. Wang, Failure modes evaluation of PV module via materials degradation approach, *Energy Procedia* 33 (2013) 256–264, <http://dx.doi.org/10.1016/j.egypro.2013.05.066>, URL: <https://www.sciencedirect.com/science/article/pii/S1876610213000763>.
- [15] N. Kim, H. Kang, K.J. Hwang, C. Han, W.S. Hong, D. Kim, E. Lyu, H. Kim, Study on the degradation of different types of backsheets used in PV module under accelerated conditions, *Sol. Energy Mater.* 120 (2014) 543–548, <http://dx.doi.org/10.1016/j.solmat.2013.09.036>, URL: <https://www.sciencedirect.com/science/article/pii/S092702481300514X>.
- [16] W. Gambogi, Y. Heta, H. Hashimoto, J. Kopchick, T. Felder, S. MacMaster, A. Bradley, B. Hamzavaytehraney, V. Felix, T. Aoki, K. Stika, L. Garreau-Illis, T.J. Trout, Weathering and durability of PV backsheets and impact on PV module performance, in: *Reliability of Photovoltaic Cells, Modules, Components, and Systems VI*, vol. 8825, SPIE, 2013, pp. 80–90, <http://dx.doi.org/10.1117/12.2024491>, URL: <https://www.spiedigitallibrary.org/conference-proceedings-of-spie/8825/88250B/Weathering-and-durability-of-PV-backsheets-and-impact-on-PV/10.1117/12.2024491.full>.
- [17] F. Liu, L. Jiang, S. Yang, Ultra-violet degradation behavior of polymeric backsheets for photovoltaic modules, *Sol. Energy* 108 (2014) 88–100, <http://dx.doi.org/10.1016/j.solener.2014.06.027>, URL: <https://www.sciencedirect.com/science/article/pii/S0038092X14003260>.
- [18] M.A.K. Jansen, A.L. Andradý, P.W. Barnes, R. Busquets, L.E. Revell, J.F. Bornman, P.J. Aucamp, A.F. Bais, A.T. Banaszak, G.H. Bernhard, L.S. Bruckman, D.P. Häder, M.L. Hanson, A.M. Heikkilä, S. Hylander, R.M. Lucas, R. Mackenzie, S. Madronich, P.J. Neale, R.E. Neale, C.M. Olsen, R. Ossola, K.K. Pandey, I. Petropavlovskikh, S.A. Robinson, T.M. Robson, K.C. Rose, K.R. Solomon, M.P. Sulbæk Andersen, B. Sulzberger, T.J. Wallington, Q.W. Wang, S.-Å. Wängberg, C.C. White, A.R. Young, R.G. Zepp, L. Zhu, Environmental plastics in the context of UV radiation, climate change, and the montreal protocol, *Global Change Biol.* 30 (4) (2024) e17279, <http://dx.doi.org/10.1111/gcb.17279>.
- [19] DuPont, Global-Field-Reliability-Report-2020.pdf, URL: <https://www.dupont.com/content/dam/dupont/amer/us/en/photovoltaic/public/documents/Global-Field-Reliability-Report-2020.pdf>.
- [20] M. Quintana, D. King, F. Hosking, J. Kratochvil, R. Johnson, B. Hansen, N. Dhare, M. Pandit, Diagnostic analysis of silicon photovoltaic modules after 20-year field exposure, in: *Conference Record of the Twenty-Eighth IEEE Photovoltaic Specialists Conference - 2000* (Cat. No.00CH37036), (ISSN: 0160-8371) 2000, pp. 1420–1423, <http://dx.doi.org/10.1109/PVSC.2000.916159>.
- [21] J.H. Wohlgemuth, D.W. Cunningham, P. Monus, J. Miller, A. Nguyen, Long term reliability of photovoltaic modules, in: 2006 IEEE 4th World Conference on Photovoltaic Energy Conference, Vol. 2, (ISSN: 0160-8371) 2006, pp. 2050–2053, <http://dx.doi.org/10.1109/WCPEC.2006.279905>.
- [22] R.J. Wieser, Y. Wang, A. Fairbrother, S. Napoli, A.W. Hauser, S. Julien, X. Gu, G.S. O'Brien, K.T. Wan, L. Ji, M.D. Kempe, K.P. Boyce, L.S. Bruckman, Field retrieved photovoltaic backsheet survey from diverse climate zones: Analysis of degradation patterns and phenomena, *Sol. Energy* 259 (2023) 49–62, <http://dx.doi.org/10.1016/j.solener.2023.04.061>, URL: <https://www.sciencedirect.com/science/article/pii/S0038092X230003079>.
- [23] C. Buerhop-Lutz, O. Stroyuk, T. Pickel, T. Winkler, J. Hauch, I.M. Peters, PV modules and their backsheets - a case study of a multi-MW PV power station, *Sol. Energy Mater. Sol. Cells* 231 (2021) 111295, <http://dx.doi.org/10.1016/j.solmat.2021.111295>, URL: <https://www.sciencedirect.com/science/article/pii/S0927024821003378>.
- [24] D.C. Miller, M. Owen-Bellini, P.L. Hacke, Use of indentation to study the degradation of photovoltaic backsheets, *Sol. Energy Mater. Sol. Cells* 201 (2019) 110082, <http://dx.doi.org/10.1016/j.solmat.2019.110082>.
- [25] M. Owen-Bellini, S.L. Moffitt, A. Sinha, A.M. Maes, J.J. Meert, T. Karin, C. Takacs, D.R. Jenket, J.Y. Hartley, D.C. Miller, P. Hacke, L.T. Schelhas, Towards validation of combined-accelerated stress testing through failure analysis of polyamide-based photovoltaic backsheets, *Sci. Rep.* 11 (1) (2021) 2019, <http://dx.doi.org/10.1038/s41598-021-81381-7>, URL: <https://www.nature.com/articles/s41598-021-81381-7>, Bandiera\_abtest: a Cc\_license\_type: cc-by Cg\_type: Nature Research Journals Number: 1 Primary\_atype: Research Publisher: Nature Publishing Group Subject\_term: Chemistry;Energy science and technology;Materials science;Mathematics and computing Subject\_term\_id: chemistry;energy-science-and-technology;materials-science;mathematics-and-computing.
- [26] Y. Wang, W.H. Huang, A. Fairbrother, L.S. Fridman, A.J. Curran, N.R. Wheeler, S. Napoli, A.W. Hauser, S. Julien, X. Gu, G.S. O'Brien, K.T. Wan, L. Ji, M.D. Kempe, K.P. Boyce, R.H. French, L.S. Bruckman, Generalized spatio-temporal model of backsheet degradation from field surveys of photovoltaic modules, *IEEE J. Photovoltaics* 9 (5) (2019) 1374–1381, <http://dx.doi.org/10.1109/JPHOTOV.2019.2928700>, Conference Name: IEEE Journal of Photovoltaics.
- [27] D.A. Gordon, Z. Zhan, L.S. Bruckman, Characterizing the weathering induced degradation of Poly(ethylene-terephthalate) using PARAFAC modeling of fluorescence spectra, *Polym. Degrad. Stab.* 161 (2019) 85–94, <http://dx.doi.org/10.1016/j.polydegradstab.2019.01.006>, URL: <https://www.sciencedirect.com/science/article/pii/S0141391019300126>.
- [28] J. Liu, A.J. Curran, J.S. Fada, X. Ma, W. Huang, C.B. Jones, E. Schnabel, M. Kohl, J.L. Braid, R.H. French, Cross-correlation analysis of the indoor accelerated and real world exposed photovoltaic systems across multiple climate zones, in: 2018 IEEE 7th World Conference on Photovoltaic Energy Conversion (WCPEC) (a Joint Conference of 45th IEEE PVSC, 28th PVSEC 34th EU PVSEC), 2018, pp. 3949–3954, <http://dx.doi.org/10.1109/PVSC.2018.8547840>.
- [29] A. Fairbrother, M. Boyd, Y. Lyu, J. Avenet, P. Illich, Y. Wang, M. Kempe, B. Dougherty, L. Bruckman, X. Gu, Differential degradation patterns of photovoltaic backsheets at the array level, *Sol. Energy* 163 (2018) 62–69, <http://dx.doi.org/10.1016/j.solener.2018.01.072>, URL: <https://www.sciencedirect.com/science/article/pii/S0038092X18300938>.
- [30] F. Rubel, K. Brugger, K. Haslinger, I. Auer, The climate of the European alps: Shift of very high resolution Köppen-Geiger climate zones 1800–2100, *Meteorol. Z.* (2016) <http://dx.doi.org/10.1127/metz/2016/0816>.
- [31] R.J. Wieser, A.S. Xin, R.H. French, L.S. Bruckman, Evaluation and augmentation of Köppen-Geiger climate zone based off of real-world satellite weather data, in: 2020 47th IEEE Photovoltaic Specialists Conference, PVSC, (ISSN: 0160-8371) 2020, pp. 1423–1428, <http://dx.doi.org/10.1109/PVSC45281.2020.9300593>, tex.ids=raymondjwieserEvaluationPredictionKoeppen2020.
- [32] T. Karin, C. Jones, A. Jain, Photovoltaic degradation climate zones, 2019, <http://dx.doi.org/10.1109/PVSC40753.2019.8980831>.
- [33] J. Ascencio-Vásquez, K. Brecl, M. Topič, Methodology of Köppen-Geiger-Photovoltaic climate classification and implications to worldwide mapping of PV system performance, *Sol. Energy* 191 (2019) 672–685, <http://dx.doi.org/10.1016/j.solener.2019.08.072>.
- [34] Z. Li, R. Wieser, X. Yu, L. Bruckman, Real world backsheets, 2020, <http://dx.doi.org/10.17605/OSF.IO/9EQBM>, URL: <https://osf.io/9eqbm/>. Publisher: OSF.
- [35] F. Faul, E. Erdfelder, A.G. Lang, A. Buchner, G\*power 3: A flexible statistical power analysis program for the social, behavioral, and biomedical sciences, *Behav. Res. Methods* 39 (2) (2007) 175–191, <http://dx.doi.org/10.3758/BF03193146>.
- [36] F. Faul, E. Erdfelder, A. Buchner, A.G. Lang, Statistical power analyses using G\*Power 3.1: Tests for correlation and regression analyses, *Behav. Res. Methods* 41 (4) (2009) 1149–1160, <http://dx.doi.org/10.3758/BRM.41.4.1149>.
- [37] M. Drobot, Z. Persin, L. Zemljic, T. Mohan, K. Stana-Kleinschek, A. Doliška, M. Bračič, V. Ribitsch, V. Harabagiu, S. Coseri, Chemical modification and characterization of poly(ethylene terephthalate) surfaces for collagen immobilization, *Central Eur. J. Chem.* 11 (2013) 1786–1798, <http://dx.doi.org/10.2478/s11532-013-0319-z>.
- [38] K.C. Cole, J. Guèvremont, A. Aji, M.M. Dumoulin, Characterization of surface orientation in poly(ethylene terephthalate) by front-surface reflection infrared spectroscopy, *Appl. Spectrosc.* 48 (12) (1994) 1513–1521, <http://dx.doi.org/10.1366/0003702944027877>, URL: <http://journals.sagepub.com/doi/10.1366/0003702944027877>.
- [39] X. Gu, C.A. Michaels, D. Nguyen, Y.C. Jean, J.W. Martin, T. Nguyen, Surface and interfacial properties of PVDF/acrylic copolymer blends before and after UV exposure, *Appl. Surf. Sci.* 252 (14) (2006) 5168–5181, <http://dx.doi.org/10.1016/j.apsusc.2005.07.051>, URL: <https://www.sciencedirect.com/science/article/pii/S0169433205010627>.
- [40] X. Cai, T. Lei, D. Sun, L. Lin, A critical analysis of the  $\alpha$ ,  $\beta$  and  $\gamma$  phases in poly(vinylidene fluoride) using FTIR, *RSC Adv.* 7 (25) (2017) 15382–15389, <http://dx.doi.org/10.1039/C7RA01267E>, URL: <https://pubs.rsc.org/en/content/articlelanding/2017/ra/c7ra01267e>. Publisher: The Royal Society of Chemistry.
- [41] S. Mohamadi, Preparation and characterization of PVDF/PMMA/Graphene polymer blend nanocomposites by using ATR-FTIR technique, 2012, <http://dx.doi.org/10.5772/36497>.
- [42] K. Foroutani, B. Pourabbas, M. Sharif, M. Mohammadzadeh, M. Fallahian, S. Khademi, Preparation of conductive flexible films by in situ deposition of polythiophene nanoparticles on polyethylene naphthalate, *Mater. Sci. Semicond. Process.* 18 (2014) 6–14, <http://dx.doi.org/10.1016/j.mssp.2013.10.015>, URL: <https://www.sciencedirect.com/science/article/pii/S1369800113003090>.
- [43] J.W. Hong, J.B. Lando, J.L. Koenig, S.H. Chough, S. Krimm, Normal-mode analysis of infrared and Raman spectra of poly(vinyl fluoride), *Vib. Spectrosc.* 3 (1) (1992) 55–66, [http://dx.doi.org/10.1016/0924-2031\(92\)85024-U](http://dx.doi.org/10.1016/0924-2031(92)85024-U), URL: <https://www.sciencedirect.com/science/article/pii/092420319285024U>.
- [44] I. Donelli, G. Freddi, V.A. Nierstrasz, P. Taddei, Surface structure and properties of poly-(ethylene terephthalate) hydrolyzed by alkali and cutinase, *Polym. Degrad. Stab.* 95 (9) (2010) 1542–1550, <http://dx.doi.org/10.1016/j.polydegradstab.2010.06.011>, URL: <https://www.sciencedirect.com/science/article/pii/S0141391010002478>.
- [45] N. Vasanthan, D.R. Salem, FTIR spectroscopic characterization of structural changes in polyamide-6 fibers during annealing and drawing, *J. Polym. Sci. Part B: Polym. Phys.* 39 (5) (2001) 536–547, [http://dx.doi.org/10.1002/1099-0488\(20010301\)39:5<536::AID-POLB1027>3.0.CO;2-8](http://dx.doi.org/10.1002/1099-0488(20010301)39:5<536::AID-POLB1027>3.0.CO;2-8), URL: [https://onlinelibrary.wiley.com/doi/abs/10.1002/1099-0488\(20010301\)39:5<536::AID-POLB1027>3.0.CO;2-8](https://onlinelibrary.wiley.com/doi/abs/10.1002/1099-0488(20010301)39:5<536::AID-POLB1027>3.0.CO;2-8), eprint: [https://onlinelibrary.wiley.com/doi/pdf/10.1002/1099-0488\(20010301\)39:5<536::AID-POLB1027>3.0.CO;2-8](https://onlinelibrary.wiley.com/doi/pdf/10.1002/1099-0488(20010301)39:5<536::AID-POLB1027>3.0.CO;2-8).

- [46] C. Slim, E. Ratajová, S. Griveau, F. Kanoufi, D. Ferraro, C. Perréard, F. d'Orlyé, A. Varenne, F. Bedioui, Two-step local functionalization of fluoropolymer Dyneon THV microfluidic materials by scanning electrochemical microscopy combined to click reaction, *Electrochem. Commun.* 60 (2015) 5–8, <http://dx.doi.org/10.1016/j.elecom.2015.07.019>, URL: <https://www.sciencedirect.com/science/article/pii/S138824811500199X>.
- [47] ASTM standard, ASTM E313-20, Standard Practice for Calculating Yellowness and Whiteness Indices from Instrumentally Measured Color Coordinates, Technical Report, ASTM International, West Conshohocken, PA, 2020, <http://dx.doi.org/10.1520/E0313-20>.
- [48] ASTM standard, ASTM D2457-21, Standard Test Method for Specular Gloss of Plastic Film and Solid Plastics, Technical Report, ASTM International, West Conshohocken, PA, 2021, <http://dx.doi.org/10.1520/D2457-21>.
- [49] S. Julien, J. Kim, Y. Lyu, D. Miller, X. Gu, K. tak Wan, Cohesive and adhesive degradation in PET-based photovoltaic backsheets subjected to ultraviolet accelerated weathering, *Sol. Energy* 224 (2021) 637–649, <http://dx.doi.org/10.1016/j.solener.2021.04.065>, Publisher Copyright: 2021 International Solar Energy Society.
- [50] O. Stroyuk, C. Buerhop-Lutz, A. Vetter, J. Hepp, J. Hauch, I.M. Peters, C.J. Brabec, Distinguishing between different types of multi-layered PET-based backsheets of PV modules with near-infrared spectroscopy, *Prog. Photovolt., Res. Appl.* 30 (8) (2022) 859–868, <http://dx.doi.org/10.1002/pip.3465>, URL: <https://onlinelibrary.wiley.com/doi/abs/10.1002/pip.3465>.
- [51] G.D. Lorenzo, R. Araneo, M. Mitolo, A. Niccolai, F. Grimaccia, Review of O&M practices in PV plants: Failures, solutions, remote control, and monitoring tools, *IEEE J. Photovoltaics* 10 (4) (2020) 914–926, <http://dx.doi.org/10.1109/JPHOTOV.2020.2994531>.
- [52] A. Peinado Gonzalo, A. Pliego Marugán, F.P. García Márquez, Survey of maintenance management for photovoltaic power systems, *Renew. Sustain. Energy Rev.* 134 (2020) 110347, <http://dx.doi.org/10.1016/j.rser.2020.110347>, URL: <https://www.sciencedirect.com/science/article/pii/S1364032120306353>.
- [53] R.J. Wieser, Z.Z. Li, S.L. Moffitt, R. Zabalza, E. Boucher, S. Ayala, M. Brown, X. Gu, L. Ji, C. O'Brien, A.W. Hauser, G.S. O'Brien, X. Yu, R.H. French, M.D. Kempe, J. Tracy, K.R. Choudhury, W.J. Gambogi, L.S. Bruckman, K.P. Boyce, Spatiotemporal modeling of real world backsheets field survey data: Hierarchical (multilevel) generalized additive models, in: 2022 IEEE 49th Photovoltaics Specialists Conference, PVSC, 2022, pp. 0255–0260, <http://dx.doi.org/10.1109/PVSC48317.2022.9938576>.
- [54] J.C. Blakesley, G. Koutsourakis, D.E. Parsons, N.A. Mica, S. Balasubramanyam, M.G. Russell, Sourcing albedo data for bifacial PV systems in complex landscapes, *Sol. Energy* 266 (2023) 112144, <http://dx.doi.org/10.1016/j.solener.2023.112144>.
- [55] S.A. Pelaez, C. Deline, P. Greenberg, J.S. Stein, R.K. Kostuk, Model and validation of single-axis tracking with bifacial PV, *IEEE J. Photovoltaics* 9 (3) (2019) 715–721, <http://dx.doi.org/10.1109/JPHOTOV.2019.2892872>.
- [56] S. Ayala Pelaez, C. Deline, Bifacial\_radiance: A python package for modeling bifacial solar photovoltaic systems, *J. Open Source Softw.* 5 (50) (2020) 1865, <http://dx.doi.org/10.21105/joss.01865>.
- [57] P. Sánchez-Friera, M. Piliouguine, J. Peláez, J. Carretero, M. Sidrach de Cardona, Analysis of degradation mechanisms of crystalline silicon PV modules after 12 years of operation in Southern Europe, *Prog. Photovolt., Res. Appl.* 19 (6) (2011) 658–666, <http://dx.doi.org/10.1002/pip.1083>, URL: <https://onlinelibrary.wiley.com/doi/abs/10.1002/pip.1083>, eprint: <https://onlinelibrary.wiley.com/doi/pdf/10.1002/pip.1083>.
- [58] G. Oreski, C. Barretta, A. Macher, G. Eder, L. Neumaier, M. Feichtner, M. Aarnio-Winterhof, Investigation of the crack propensity of co-extruded polypropylene backsheets for photovoltaic modules, *Sol. Energy Mater. Sol. Cells* 259 (2023) 112438, <http://dx.doi.org/10.1016/j.solmat.2023.112438>.